

# Spatiotemporal Heterogeneity of Local Free Volumes in Highly Supercooled Liquid

Hayato Shiba\*

*Institute for Solid State Physics, University of Tokyo, Chiba 277-8581, Japan*

Takeshi Kawasaki

*Department of Physics, Kyoto University, Kyoto 606-8502, Japan*

(Dated: February 17, 2012)

We discuss the spatiotemporal behavior of local density and its relation to dynamical heterogeneity (DH) in a highly supercooled liquid by using molecular dynamics simulations of a binary mixture with different particle sizes in two dimensions. To trace voids heterogeneously existing with lower local densities, which move along with the structural relaxation, we employ the minimum local density for each particle in a time window whose width is set along with the structural relaxation time. Particles subject to free volumes correspond well to the mobile region of DH. However, no growth in the correlation length of heterogeneity in the minimum local density distribution takes place.

PACS numbers: 64.70.kj, 81.05.Kf, 61.54.Fs

The reason for the drastic slow down in dynamics when liquids are cooled toward the glass transition temperature has been a long-standing problem. In the last two decades, numerous efforts have been made to study this problem via molecular dynamics (MD) simulations[1]. The recently proposed concept of “dynamic heterogeneity” (DH) [2–6] has shown the existence of contrast between mobile and immobile regions of supercooled liquids on a large scale, as if there were critical fluctuations hidden behind. In recent literature, considerable attention has been focused on relation of DH to the structural heterogeneity of medium length-scale crystalline order[7, 8], icosahedral order[9], local potential energy[10], and so on. In the context of experiments especially on metallic, polymer, and colloidal glasses, density fluctuations have been observed over short to long lengths[11–13]. One of the primary theoretical challenges had been the construction of statistical descriptions of solids and glasses including the effects of vacancies or local-free volume[14–17]. In MD simulations of binary mixtures usually employed in studies of supercooled liquids, density fluctuations are too weak to be captured clearly[3, 8, 18], and the correlation of such fluctuations to DH has only partially been observed[19]. In two-dimensional (2D) crystals under melting, where the density fluctuation is more pronounced than in glass, the diffusion of defect clusters with relatively smaller local densities is ascribed as the cause of DH[20]. In this Letter, we clarify the relationship between the local density and DH by capturing and tracing weakly existing density fluctuations in a constructive manner.

We investigate a 2D binary mixture composed of two atomic species, 1 and 2, with  $N_1 = N_2 = 32000$  particles. The particles interact via the soft-core potentials  $v_{\alpha\beta}(r) = \epsilon(\sigma_{\alpha\beta}/r)^{12} + C_{\alpha\beta}$  where  $\sigma_{\alpha\beta} = (\sigma_\alpha + \sigma_\beta)/2$  and  $r$  denote the interaction lengths and the distance between two particles respectively, with  $\alpha, \beta \in \{1, 2\}$ .

The interaction is truncated at  $r = 4.5\sigma_1$  and a constant  $C_{\alpha\beta}$  is set so as to ensure continuity of the potential at the cutoff. The size ratio between the two species is  $\sigma_2/\sigma_1 = 1.4$  to prevent crystallization, and the mass is set as  $m_2/m_1 = (\sigma_2/\sigma_1)^2$ . The particle density is fixed at a high value of  $\phi = (N_1\sigma_1^2 + N_2\sigma_2^2)/V = 1.2$ , and therefore the particle configurations are jammed in the supercooled state. No tendency of phase separation is detected in our computation times. Space, time, and temperature are measured in units of  $\sigma_1$ ,  $\tau_0 = \sqrt{m_1\sigma_1^2/\epsilon}$ , and  $\epsilon/k_B$ , respectively. Dependence of  $\alpha$ -relaxation time on the temperature  $T$  is shown in Table I. A sufficiently long annealing time  $t_A$  is chosen ( $t_A > 30\tau_\alpha$ ) with the time step being  $\Delta t = 0.005$ . No aging effect was appreciable in the course of calculation of pressure, density time correlations, etc. After performing the above procedure at each temperature, we begin to collect the data. This time point in each of our simulations is denoted as  $t = 0$  in the following.

First, for each particle  $i$ , we define the local density by counting the particles within the distance  $\Delta r = |\mathbf{r} - \mathbf{r}_i| \leq r_0$  from  $i$

$$n_i(r_0) = \frac{1}{\pi r_0^2} \int_{\Delta r < r_0} d\mathbf{r} \sigma_j^2 \delta(\mathbf{r}_j - \mathbf{r}). \quad (1)$$

This local density is weighted by the assumed area  $\sigma_j^2$ . The inset of Fig. 1 shows the long-time average of the local density  $[n_i(r_0)]_N$  at  $T = 0.56$ . Here,  $[\mathcal{A}_i]_N = N^{-1} \sum_i \mathcal{A}_i$  denotes the average over all the particles. This quantity corresponds to a radial distribution function  $g(r_0)$  defined in a naive manner.

For the same simulation run, at appropriate time intervals, we estimate the local density in the mobile regions of DH as follows: bonds are defined at each time  $t_0$  as particle pairs between  $i$  and  $j$  satisfying  $r_{ij}(t_0) \leq A_1\sigma_{\alpha\beta}$ , and after a time interval  $\Delta t$  bonds are regarded to be broken if  $r_{ij}(t_0 + \Delta t) > A_2\sigma_{\alpha\beta}$  [2, 3]. The cutoffs are

TABLE I: Dependence of  $\alpha$ -relaxation time ( $\tau_\alpha$ ) and bond-relaxation time ( $\tau_b$ ) on  $T$ .

$T$	0.56	0.64	0.72	0.80	0.96	1.20
$\tau_\alpha$	$2.14 \times 10^3$	75.5	10.5	5.39	2.86	1.47
$\tau_b$	$1.41 \times 10^5$	$1.90 \times 10^4$	$5.25 \times 10^3$	$1.87 \times 10^3$	$5.35 \times 10^2$	$1.85 \times 10^2$

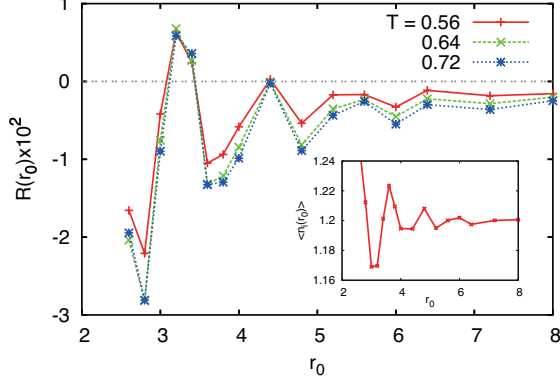


FIG. 1: Degree of deviation  $R(r_0)$  of the local densities around the broken bonds  $[n_i(r_0)]_{b.b.}$  (obtained at intervals of  $\Delta t = 2 \times 10^2$ ) from that averaged over the entire system  $[n_i(r_0)]_N$ , plotted as a function of averaging radius  $r_0$ . The data for  $T = 0.56, 0.64$ , and  $0.72$  are shown. Inset:  $\langle n_i(r_0) \rangle$  is shown for  $T = 0.56$ .

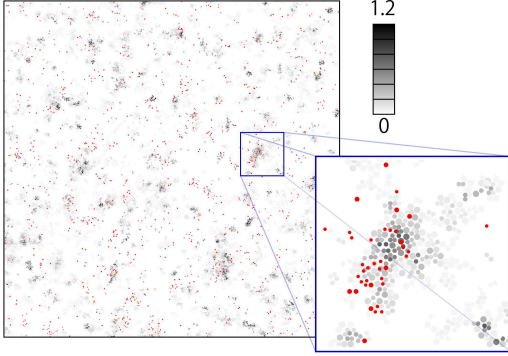


FIG. 2: The red points show the distribution of 2% of the particles having smaller local densities  $\langle n_i(r_0) \rangle_{IE}$ , which is averaged over  $t \in [0, 10]$ , in an IE of 32 runs at  $T = 0.56$ . The number distribution of broken bonds for the same IE  $\langle \mathcal{B}(\mathbf{r}, \Delta t) \rangle_{IE}$  with  $t \in [0, 122]$  is shown according to the scale bar on the right. For clarity, a magnified figure is shown on the bottom right.

set to  $A_1 = 1.15$  and  $A_2 = 1.6$ , respectively. We take the local density profile only for particles that have undergone these broken bonds for  $\Delta t = 2 \times 10^2$ , and we denote their average local density profile as  $[n_i(r_0)]_{b.b.}$ . The main graph in Fig. 1 shows the long-time average  $R(r_0, \Delta t)$  of the relative degree of deviation as given by

$$R(r_0, \Delta t) = \left( \frac{[n_i(r_0)]_{b.b.}}{[n_i(r_0)]_N} - 1 \right). \quad (2)$$

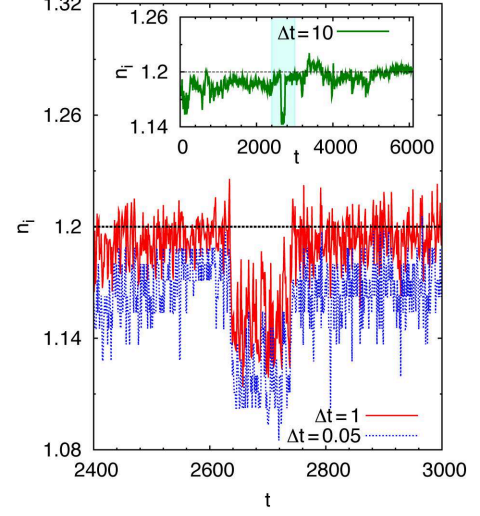


FIG. 3: The red solid line shows the local density  $n_i(r_0)$  ( $r_0 = 6.0\sigma_1$ ) averaged over every unit time ( $\Delta t_d = 1$ ) for a run at  $T = 0.56$ . On the blue dashed line,  $n_i(r_0)$  is calculated for every time interval of  $\Delta t_d = 0.05$  and each minimum is plotted per unit time. Therefore, the latter is systematically lower than the former due to thermal fluctuations on a short time scale. Inset: For the same particle and for a longer time interval,  $n_i(r_0)$  is plotted when averaged over a time interval of  $\Delta t_d = 10$ .

While  $R(r_0)$  exhibits an oscillating behavior at small values of  $r_0$  mainly due to the mixed contributions from larger and smaller components, its value is systematically lower than zero when  $r_0$  is sufficiently large. Thus, around the broken bonds. *i.e.*, in the mobile regions, the smaller local density can be characterized with a sufficiently large value of  $r_0$ . We employ  $r_0 = 6.0$  in our following discussions.

To characterize the mobile regions of DH, we count the number of broken bonds pairs for each particle as  $\mathcal{B}_i(\Delta t) = \sum_{j \in b.b.} 1$ , where the summation is taken over  $j$  particles at the broken bond ends of  $i$  particles calculated over time intervals of length  $\Delta t$ . Since DH is uniquely dependent on the particle positions[21], isoconfigurational ensembles (IEs) of 32 runs are employed and an average is obtained over these runs. This IE average is denoted as  $\langle \cdot \rangle_{IE}$  in the following discussions. In Fig. 2, we demonstrate  $\langle \mathcal{B}_i(\Delta t) \rangle_{IE}$  for a short time interval,  $t \in [0, \Delta t]$  ( $\Delta t = 122$ ), together with distribution of 2% of particles having the lowest local densities  $\langle n_i(r_0) \rangle_{IE}$  taken at the initial stage  $t \in [0, 10]$ . Clusters of particles

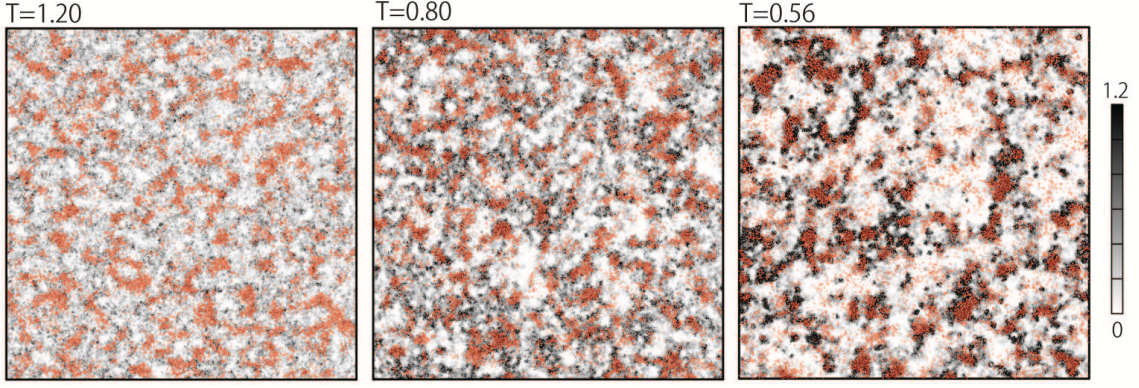


FIG. 4: The red points show the distribution of 25% of the particles having smaller values of minimum local densities  $\langle \nu_i(\Delta t_b) \rangle_{\text{IE}}$ , in an IE of 32 runs performed for  $\Delta t_b = 6, 60$ , and 6100 for  $T = 1.2, 0.80$ , and 0.56, respectively. The number distribution of broken bonds  $\langle \mathcal{B}_i(\Delta t_b) \rangle_{\text{IE}}$  is shown by the gray scale according to the scale bar on the right.

with low local densities are observed, and the particles are clustered at distances of several times the particle radius. On a mesoscopic scale, this clustering corresponds to particle propensity represented by  $\langle \hat{\mathcal{B}}(\mathbf{r}, \Delta t) \rangle_{\text{IE}}$ , with  $\hat{\mathcal{B}}(\mathbf{r}, \Delta t) = \sum_j \sigma_j^2 \mathcal{B}_j(\Delta t) \delta(\mathbf{r} - \mathbf{r}_j(0))$ . From this correspondence, a natural speculation would be that the local free volumes within each cluster interact with each other with a blurred heterogeneity and move around, thereby leading to a clear heterogeneity in the dynamics.

To understand the cluster relationship with DH, it is necessary to capture how they move over longer time intervals. For  $T = 0.56, 0.64, 0.72, 0.80, 0.96$ , and 1.20, simulation runs of IEs are performed with time intervals of  $\Delta t_b(T) = 6100, 815, 210, 80, 23$ , and 8, respectively. Upon using the concept of bond relaxation time  $\tau_b(T)$  introduced in a previous study[3] and defined by  $N_b(t_0 + \tau_b) = N_b(t_0)/e$ , these time intervals satisfy  $\Delta t_b(T) \simeq 0.043 \tau_b(T)$ . Here,  $N_b(t)$  denotes the total number of bonds at time  $t$ , and  $\tau_b(T)$  characterizes the time scale of structural relaxation (see Table I for actual values). In these intervals, almost identical portions of the total initial bonds become broken for all values of  $T$ .

At low  $T$  where slow dynamics realize, particle rearrangements agitated by the thermal fluctuations are expected to become intermittent. In Fig. 3, for  $T = 0.56$ , change in local density  $n_i$  with time is measured for one specific particle in the mobile region of DH. Averaging  $n_i$  over every time interval of  $\Delta t_d = 10$  as shown in the inset, the local density is observed to be fluctuating around  $\phi$ . In the region around  $t = 2700$ , the density reduces for a time interval of order  $10^2$  by an amount of around  $\Delta n_i \simeq 0.05$ . Interestingly, since  $\Delta n_i \times \pi(r_0/2)^2 \sim O(1)$ , this reduction corresponds to a free volume of one particle size scale for the current radius  $r_0 = 6.0$ . The lower the temperature, the longer the time interval is expected to be due to smaller thermal fluctuations. Upon decreasing the averaging time  $\Delta t_d$  to 1 and 0.05, the temporal fluctuation of  $n_i(r_0)$  appears more explicitly. In the main

graph, the red solid line represents  $n_i(r_0)$  averaged over  $\Delta t_d = 1$ . For a much shorter time interval of  $\Delta t_d = 0.05$ , we accumulate the data of the density, and for every interval of unit time length ( $\Delta t = 1$ ), we take the minimum of  $n_i(r_0)$ . The blue dashed line represents the minimum value of the local density for each unit time thus taken. Because these two lines behave in a parallel manner when the density drops down, the minimum value in the local density history assumed by one particle can well represent and characterize the general time-development of the local density.

To capture the trace of free volumes and its correspondence to DH, we investigate the spatial distribution of the “minimum local density” that is defined as

$$\hat{\nu}_i(\Delta t) = \min_{t \in [t_0, t_1]} n_i, \quad t_1 = t_0 + \Delta t. \quad (3)$$

The above term indicates the minimum value in the density history for each particle  $i$ . The IE average of  $\hat{\nu}(\mathbf{r}, \Delta t_b) = \sum_j \nu_j \delta(\mathbf{r} - \mathbf{r}_j(0))$  can illustrate the spatiotemporal heterogeneity of free volumes in an enhanced manner. Figure 4 shows the distribution of 25% of the total number of particles having lower  $\langle \nu_i(\Delta t_b) \rangle_{\text{IE}}$  mapped together with the broken bond distribution  $\langle \mathcal{B}_i(\Delta t_b) \rangle_{\text{IE}}$ . The lower the value of  $T$  is, the more distinct is the correspondence between these distributions.

Quantitatively, this correspondence is illustrated for  $T = 0.56$  in Fig. 5; the correspondence is observed as a scattered plot between  $\langle \hat{\nu}(\mathbf{r}, \Delta t_b) \rangle_{\text{IE}}$ , with  $\hat{\nu}(\mathbf{r}, \Delta t_b) = \sum_j \nu_j \delta(\mathbf{r} - \mathbf{r}_j(0))$  and  $\langle \mathcal{B}(\mathbf{r}, \Delta t_b) \rangle_{\text{IE}}$  averaged in each cell, thereby squarely dividing the total system into a  $12 \times 12$  grid of size  $(L/12)^2$ .

To examine how the heterogeneity in the density evolves, in Fig. 6, we show the structure factor of “free volume degree”  $\hat{\nu}(\mathbf{r}, \Delta t_b)$  defined as

$$S_\nu(k, \Delta t_b) = \langle |\hat{\nu}_{\mathbf{k}}(\Delta t_b)|^2 \rangle_{\text{IE}}, \quad (4)$$

where  $\delta \hat{\nu}(\mathbf{r}, \Delta t_b) = \sum_j \sigma_j^2 (\nu_j - [\nu_j]_N) \delta(\mathbf{r} - \mathbf{r}_j(0))$  is



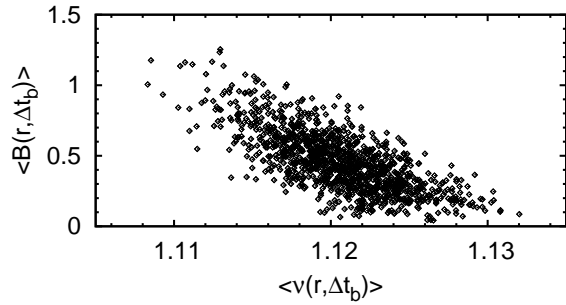


FIG. 5: Scattered plot of cell-averaged quantities between  $\langle \hat{\nu}(\mathbf{r}, \Delta t_b) \rangle_{\text{IE}}$  and  $\langle \hat{B}(\mathbf{r}, \Delta t_b) \rangle_{\text{IE}}$  for  $T = 0.56$ . The cells divide the total system into a  $12 \times 12$  grid. The data for runs with eight independent initial conditions are shown in this figure, and an IE average over 32 runs is taken for each run.

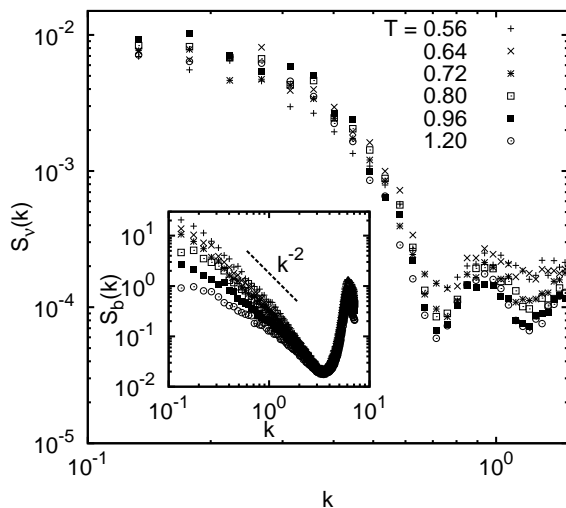


FIG. 6: Structure factor of the “free volume degree”  $S_\nu(k, \Delta t_b)$  defined in Eq. (4) for various values of  $T$ . Inset: Structure factor of the broken bonds  $S_b(k, \Delta t_b)$ , exhibiting the Ornstein-Zernike form typical to DH whose correlation length grows as  $T$  decreases.

the mesoscopic fluctuation of  $\nu_i$ , and  $\hat{\nu}_{\mathbf{k}}(\Delta t_b)$  indicates Fourier components of  $\delta \hat{\nu}(\mathbf{r}, \Delta t_b)$ . The average is taken over IEs of 32 runs generated from 32 independent initial configurations, and thus, data from 1024 runs performed over a duration of  $\Delta t_b$  are used for each  $T$ . In the inset of Fig. 6, we also show the structure factor of corresponding broken bonds

$$S_b(k, \Delta t_b) = \langle |\hat{B}_{\mathbf{k}}(\Delta t_b)|^2 \rangle_{\text{IE}} \quad (5)$$

which gives information on how DH evolves at long-wavelengths. Since one isolated free volume lowers the values of  $n_i(r_0)$  of particles within the distance of  $l = r_0 \sigma_1$ , we have a small peak of  $S_\nu(k, \Delta t_b)$  around  $k \sim 2\pi/l \simeq 10^0$ , and this peak is enhanced at long-wavelengths. Remarkably,  $S_\nu(k, \Delta t_b)$  does not change with tempera-

ture exhibiting the same degree of heterogeneity even at long-wavelengths, while  $S_b(k, \Delta t_b)$  displays the Ornstein-Zernike form with growing length scales for lower values of  $T$  in a manner similar to those obtained in previous studies[2, 3]. That is, for the interval of corresponding structural relaxation time  $\Delta t_b(T)$  the heterogeneity in  $\hat{\nu}(\mathbf{r}, \Delta t_b)$  is nearly independent of the temperature, and  $\hat{B}(\mathbf{r}, \Delta t_b)$  shown in Fig. 4 might suggest existence of other structural origins for DH; as regards the arguments on these origins in the literature, such as density gradient, growing static length scales, and so on, their relation to our results should be examined in the future.

In conclusion, we have clarified the relation between free volume distribution and DH for various temperature for the first time, using MD simulations of a binary mixture. While the distribution of free volumes is extended at a mesoscale to form clusters, within each cluster, several free volumes are scattered at the one-particle level, as shown in Fig. 2. These complex characteristics have thus far not been discussed in the literature of MD simulations of glasses. DH can be attributed to cooperative rearrangements of several free volumes in such clusters due to the effect of thermal excitations. In our binary mixture, the density distribution and the relative degrees of local density drop down at a free volume are suggested to be independent of the temperature, with no apparent length scales growing with decreasing temperature.

The authors thank A. Ikeda, K. Miyazaki, and O. Yamamuro for enlightening discussions. The numerical calculations were carried out mainly on SGI Altix ICE 8400EX system at ISSP Supercomputer Center, University of Tokyo. This work is supported by JSPS Core-to-Core Program “International research network for non-equilibrium dynamics of soft matter”. TK is supported by a Grant-in-Aid for JSPS Fellows.

\* Electronic address: shiba@issp.u-tokyo.ac.jp

- [1] K. Binder and W. Kob, *Glassy Materials and Disordered Solids* (World Scientific, Singapore, 2005).
- [2] R. Yamamoto and A. Onuki, J. Phys. Soc. Jpn. **66**, 2545 (1997).
- [3] R. Yamamoto and A. Onuki, Phys. Rev. E **58**, 3515 (1998).
- [4] W. Kob, C. Donati, S. J. Plimpton, P. H. Poole, and S. C. Glotzer, Phys. Rev. Lett. **79**, 2827 (1997).
- [5] C. Donati, J. F. Douglas, W. Kob, S. J. Plimpton, P. H. Poole, and S. C. Glotzer, Phys. Rev. Lett. **80**, 2338 (1998).
- [6] G. Biroli, J.-P. Bouchaud, K. Miyazaki, and D. R. Reichman, Phys. Rev. Lett. **97**, 195701 (2006).
- [7] T. Kawasaki, T. Araki, and H. Tanaka, Phys. Rev. Lett. **99**, 215701 (2007).
- [8] H. Tanaka, T. Kawasaki, H. Shintani, and K. Watanabe, Nat Mater **9**, 324 (2010).
- [9] M. Dzугutov, S. I. Simdyankin, and F. H. M. Zetterling,

- Phys. Rev. Lett. **89**, 195701 (2002).
- [10] G. S. Matharoo, M. S. G. Razul, and P. H. Poole, Phys. Rev. E **74**, 050502(R) (2006).
  - [11] E. W. Fischer, G. Meier, T. Rabenau, A. Patkowski, W. Steffen, and W. Thönnies, J. Non-Cryst. Solids **131-133**, 134 (1991).
  - [12] W. van Meegen and P. N. Pusey, Phys. Rev. A **43**, 5429 (1991).
  - [13] T. Kanaya, A. Patkowski, E. W. Fischer, J. Seils, H. Gläser, and K. Kaji, Acta Polymer. **45**, 137 (1994).
  - [14] M. H. Cohen and D. Turnbull, J. Chem. Phys. **31**, 1164 (1959).
  - [15] P. D. Flemming-III and C. Cohen, Phys. Rev. B **13**, 500 (1976).
  - [16] A. S. Argon, Acta Metal. **27**, 47 (2009).
  - [17] A. Onuki, A. Furukawa, and A. Minami, PRAMANA - J. Phys. **64**, 661 (2005).
  - [18] A. Widmer-Cooper and P. Harrowell, J. Non-Cryst. Solids **352**, 5098 (2006).
  - [19] I. Ladadwa and H. Teichler, Phys. Rev. E **73**, 031501 (2006).
  - [20] H. Shiba, A. Onuki, and T. Araki, EPL **86**, 66004 (2009).
  - [21] A. Widmer-Cooper, P. Harrowell, and H. Fynewever, Phys. Rev. Lett. **93**, 135701 (2004).